

Modeling and Control of DC-DC Converters

Shen, Yanfeng; Qin, Zian; Wang, Huai

DOI

[10.1016/B978-0-12-805245-7.00003-2](https://doi.org/10.1016/B978-0-12-805245-7.00003-2)

Publication date

2018

Document Version

Final published version

Published in

Control of Power Electronic Converters and Systems

Citation (APA)

Shen, Y., Qin, Z., & Wang, H. (2018). Modeling and Control of DC-DC Converters. In F. Blaabjerg (Ed.), *Control of Power Electronic Converters and Systems* (pp. 69-92). Academic Press. <https://doi.org/10.1016/B978-0-12-805245-7.00003-2>

Important note

To cite this publication, please use the final published version (if applicable). Please check the document version above.

Copyright

Other than for strictly personal use, it is not permitted to download, forward or distribute the text or part of it, without the consent of the author(s) and/or copyright holder(s), unless the work is under an open content license such as Creative Commons.

Takedown policy

Please contact us and provide details if you believe this document breaches copyrights. We will remove access to the work immediately and investigate your claim.

Modeling and Control of DC-DC Converters

Yanfeng Shen*, Zian Qin[†] and Huai Wang*

*Aalborg University, Aalborg, Denmark, [†]Delft University of Technology, Delft, The Netherlands

3.1 FREQUENCY-DOMAIN VOLTAGE-MODE CONTROL OF A BUCK DC-DC CONVERTER

3.1.1 Specifications of the Buck DC-DC Converter

The circuit diagram of the Buck DC-DC converter is shown in Fig. 3.1. The input voltage $V_{in}=110\text{ V}$, the output voltage $V_o=48\text{ V}$, the nominal output power $P_{oN}=500\text{ W}$, the switching frequency $f_s=100\text{ kHz}$, the maximum current ripple in the output inductor $\Delta I_{L_o}=10\% I_o$, and the maximum output voltage ripple $\Delta V_o=0.5\% V_o$. For an output voltage of 48 V , the corresponding duty cycle $D=V_o/V_{in}=48\text{ V}/110\text{ V}=0.44$ and the output current $I_o=500\text{ W}/48\text{ V}=10.42\text{ A}$. Based on the specifications, the required output inductance L_o and output capacitance C_o can be obtained

$$L_o \geq \frac{(1-D)T_s V_o}{\Delta I_{L_o}} = \frac{(1-0.44) \times 10 \times 10^{-6} \times 48}{0.1 \times 10.42} = 258 \mu\text{H} \quad (3.1)$$

$$C_o \geq \frac{\Delta I_{L_o} T_s}{8 \Delta V_o} = \frac{1.042 \times 10 \times 10^{-6}}{8 \times 0.24} = 5.43 \mu\text{H} \quad (3.2)$$

In practice, the output inductor $L_o=260\mu\text{H}$ and the output capacitor $C_o=220\mu\text{F}$. The equivalent series resistances (ESRs) of the output inductor and capacitor are $R_{L_o}=0.1\ \Omega$ and $R_{C_o}=0.2\ \Omega$, respectively.

3.1.2 Small-Signal Modeling of Buck DC-DC Converter

The operation principle of the Buck converter is simple: when the switch S is turned-on, the input source V_{in} supplies power to the load through the output inductor L_o and output capacitor C_o , as shown in Fig. 3.2A when S is turned-off, the inductor L_o and output capacitor C_o release energy to the load via the freewheeling diode D , as shown in Fig. 3.2B. The duty cycle of S being

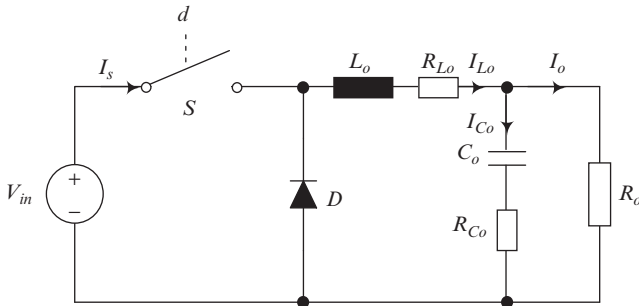


FIG. 3.1 Circuit diagram of the buck DC-DC converter.

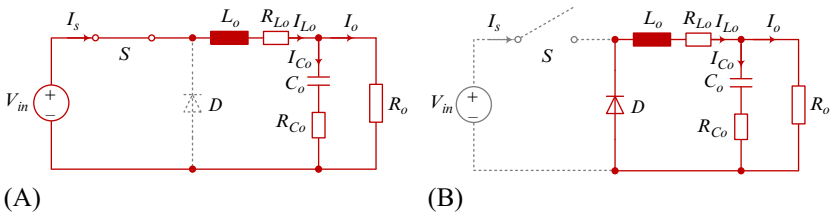


FIG. 3.2 Equivalent circuit of the Buck dc-dc converter when the switch S is (A) turned-on or (B) turned-off.

turned-on is denoted as d and then that of S being off is $1 - d$ if the deadtime is neglected. According to the Kirchhoff's current and Kirchhoff's voltage laws, the basic differential equations can be derived for the two states.

State I ($t \in [0, dT_s]$), switch S is turned on:

$$\begin{cases} L_o \frac{di_{L_o}}{dt} = v_{in} - v_o - R_{L_o}i_{L_o} \\ C_o \frac{dv_{C_o}}{dt} = i_{L_o} - i_o \\ v_o = v_{C_o} + R_{C_o}(i_{L_o} - i_o) \end{cases} \quad (3.3)$$

State II ($t \in [dT_s, T_s]$), switch S is turned off:

$$\begin{cases} L_o \frac{di_{L_o}}{dt} = -v_o - R_{L_o}i_{L_o} \\ C_o \frac{dv_{C_o}}{dt} = i_{L_o} - i_o \\ v_o = v_{C_o} + R_{C_o}(i_{L_o} - i_o) \end{cases} \quad (3.4)$$

The time durations for states I and II are dT_s and $(1 - d)T_s$, respectively. In the meanwhile, the state variables (i.e., the inductor current i_{L_o} and the capacitor voltage v_{C_o}) and the output variable (i.e., the output voltage v_o) are continuous

in time. Therefore, the averaged differential equations over one switching cycle can be obtained as follows

$$\begin{cases} L_o \frac{di_{L_o}}{dt} = dv_{in} - v_o - R_{L_o} i_{L_o} \\ C_o \frac{dv_{C_o}}{dt} = i_{L_o} - i_o \\ v_o = v_{C_o} + R_{C_o} (i_{L_o} - i_o) \end{cases} \quad (3.5)$$

As can be seen from Eq. (3.5) that there is a term dv_{in} which is a product of the input variable v_{in} and the control variable d . That is the averaged model is nonlinear, and therefore the controller cannot be designed with the classical control theory. In order to obtain a linear model, perturbations at the steady-state operation (equilibrium) point should be performed. In this way, each variable contains a DC term (i.e., the steady-state operation point) and a small AC term, i.e., $i_{L_o} = I_{L_o} + \tilde{i}_{L_o}$, $v_{C_o} = V_{C_o} + \tilde{v}_{C_o}$, $v_o = V_o + \tilde{v}_o$, $i_o = I_o + \tilde{i}_o$, $v_{in} = V_{in} + \tilde{v}_{in}$, and $d = D + \tilde{d}$. Substituting them into Eq. (3.5) yields

$$\begin{cases} L_o \frac{d}{dt} (I_{L_o} + \tilde{i}_{L_o}) = (D + \tilde{d}) (V_{in} + \tilde{v}_{in}) - (V_o + \tilde{v}_o) - R_{L_o} (I_{L_o} + \tilde{i}_{L_o}) \\ C_o \frac{d}{dt} (V_{C_o} + \tilde{v}_{C_o}) = (I_{L_o} + \tilde{i}_{L_o}) - (I_o + \tilde{i}_o) \\ (V_o + \tilde{v}_o) = (V_{C_o} + \tilde{v}_{C_o}) + R_{C_o} [(I_{L_o} + \tilde{i}_{L_o}) - (I_o + \tilde{i}_o)] \end{cases} \quad (3.6)$$

Applying the steady-state differential equation and neglecting the second-order terms, Eq. (3.6) can be simplified as linear small-signal AC equations

$$\begin{cases} L_o \frac{d}{dt} \tilde{i}_{L_o} = D \tilde{v}_{in} + \tilde{d} V_{in} - \tilde{v}_o - R_{L_o} \tilde{i}_{L_o} \\ C_o \frac{d}{dt} \tilde{v}_{C_o} = \tilde{i}_{L_o} - \tilde{i}_o \\ \tilde{v}_o = \tilde{v}_{C_o} + R_{C_o} (\tilde{i}_{L_o} - \tilde{i}_o) \end{cases} \quad (3.7)$$

Performing Laplace transform to Eq. (3.7) yields its frequency-domain form, i.e.,

$$\begin{cases} sL_o \tilde{i}_{L_o}(s) = D \tilde{v}_{in}(s) + \tilde{d}(s) V_{in} - \tilde{v}_o(s) - R_{L_o} \tilde{i}_{L_o}(s) \\ sC_o \tilde{v}_{C_o}(s) = \tilde{i}_{L_o}(s) - \tilde{i}_o(s) \\ \tilde{v}_o(s) = \tilde{v}_{C_o}(s) + R_{C_o} [\tilde{i}_{L_o}(s) - \tilde{i}_o(s)] \end{cases} \quad (3.8)$$

Eliminate $v_{C_o}(s)$ and $i_{L_o}(s)$ in Eq. (3.8), and $\tilde{v}_o(s)$ can be obtained:

$$\tilde{v}_o(s) = \frac{[D \tilde{v}_{in}(s) + V_{in} \tilde{d}(s) - R_{L_o} \tilde{i}_o(s) - sL_o \tilde{i}_o(s)] \cdot (1 + sR_{C_o} C_o)}{1 + sC_o (R_{C_o} + R_{L_o}) + s^2 C_o L_o} \quad (3.9)$$

Then different small-signal transfer functions can be derived with Eq. (3.9)

$$\begin{aligned}
 G_{d2v_o} &= \left. \frac{\tilde{v}_o(s)}{\tilde{d}(s)} \right|_{\tilde{v}_{in}(s)=0, \tilde{i}_o(s)=0} = \frac{V_{in}(1+sR_{C_o}C_o)}{1+sC_o(R_{C_o}+R_{L_o})+s^2C_oL_o} \\
 G_{v_{in}2v_o} &= \left. \frac{\tilde{v}_o(s)}{\tilde{v}_{in}(s)} \right|_{\tilde{d}(s)=0, \tilde{i}_o(s)=0} = \frac{D(1+sR_{C_o}C_o)}{1+sC_o(R_{C_o}+R_{L_o})+s^2C_oL_o} \\
 G_{i_o2v_o} &= \left. \frac{\tilde{v}_o(s)}{\tilde{i}_o(s)} \right|_{\tilde{d}(s)=0, \tilde{v}_{in}(s)=0} = \frac{-(R_{L_o}+sL_o) \cdot (1+sR_{C_o}C_o)}{1+sC_o(R_{C_o}+R_{L_o})+s^2C_oL_o}
 \end{aligned} \tag{3.10}$$

3.1.3 Voltage-Model Controller Design of Buck DC-DC Converter

The PI controller can be expressed as

$$G_{PI}(s) = K_p \left(1 + \frac{K_I}{s} \right) \tag{3.11}$$

The system switching frequency $\omega_s = 628.32 \text{ krad/s}$. The bode plot of the control-to-output transfer function is shown in Fig. 3.3. As can be observed,

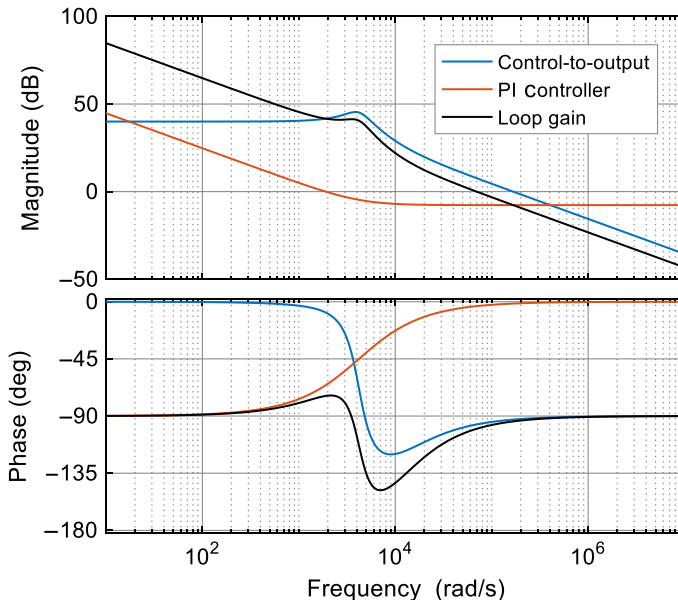


FIG. 3.3 Bode plot of the control-to-output transfer function, the PI controller, and the loop gain.

there are two corner frequencies, 4.21 and 8.35 krad/s, and the crossover frequency is 167 krad/s. In the meanwhile, the crossover frequency of the open-loop transfer function should not be higher than 1/10 to 1/5 of the switching frequency. In this case, the crossover ω_c is set as 1/9 of the switching frequency, i.e., ω_c should be corrected to be about 69.8 krad/s.

The gain of the control-to-output transfer function at $\omega_c = 69.8$ krad/s is 7.69 dB. Therefore, the required gain from the PI compensator should be $K_p = -7.69$ dB = 0.4126. The corner frequency of the PI controller should approximately correspond to the first corner frequency of the control-to-output transfer function. Thus, $K_I = \omega_I = 4.21$ krad/s.

The transfer functions of both the PI controller and the open-loop gain are depicted in Fig. 3.3 as well. As can be seen, the open-loop transfer function has been corrected with the crossover frequency $\omega_c = 69.8$ krad/s and the phase margin being equal to 80° . The bode plots of open-loop and closed-loop transfer functions are shown in Fig. 3.4. It can be observed that the high loop gain results in a strong suppression of disturbances.

3.1.4 Simulation Results of the Case Study

The closed-loop results from the circuit simulation and the small-signal model are shown in Figs. 3.5–3.7. Both the analytical modeling and simulation results are based on the specific case study described in Section 3.1.1. As can be seen, the developed small-signal model and the designed controller can predict both the dynamic and static performances of the Buck DC-DC converter with negligible error compared to simulations. When the output voltage reference is changed from 48 to 49 V, the PI controller helps the system to track the reference tightly, as shown in Fig. 3.5. When the perturbations (i.e., the input voltage in Fig. 3.6 and the load in Fig. 3.7) appear, their impact on the output voltage can be effectively attenuated.

3.2 FREQUENCY-DOMAIN CURRENT-MODE CONTROL OF A BOOST DC-DC CONVERTER

3.2.1 Specifications of the Boost DC-DC Converter

The circuit diagram of a current mode-controlled (CMC) Boost DC-DC converter is shown in Fig. 3.8. The input voltage $v_i = 150$ V, the output voltage $v_o = 350$ V, the nominal output power $P_o = 2$ kW, the switching frequency $f_s = 50$ kHz, and the maximum current ripple in the input inductor L is limited to 25%. An inductor with inductance $L = 514$ μ H and ESR $R_L = 0.02$ Ω is selected. The output capacitor $C = 450$ μ F and its ESR $R_C = 0.01$ Ω . The current sensor resistor R_s shown in Fig. 3.8 is 0.2 Ω .

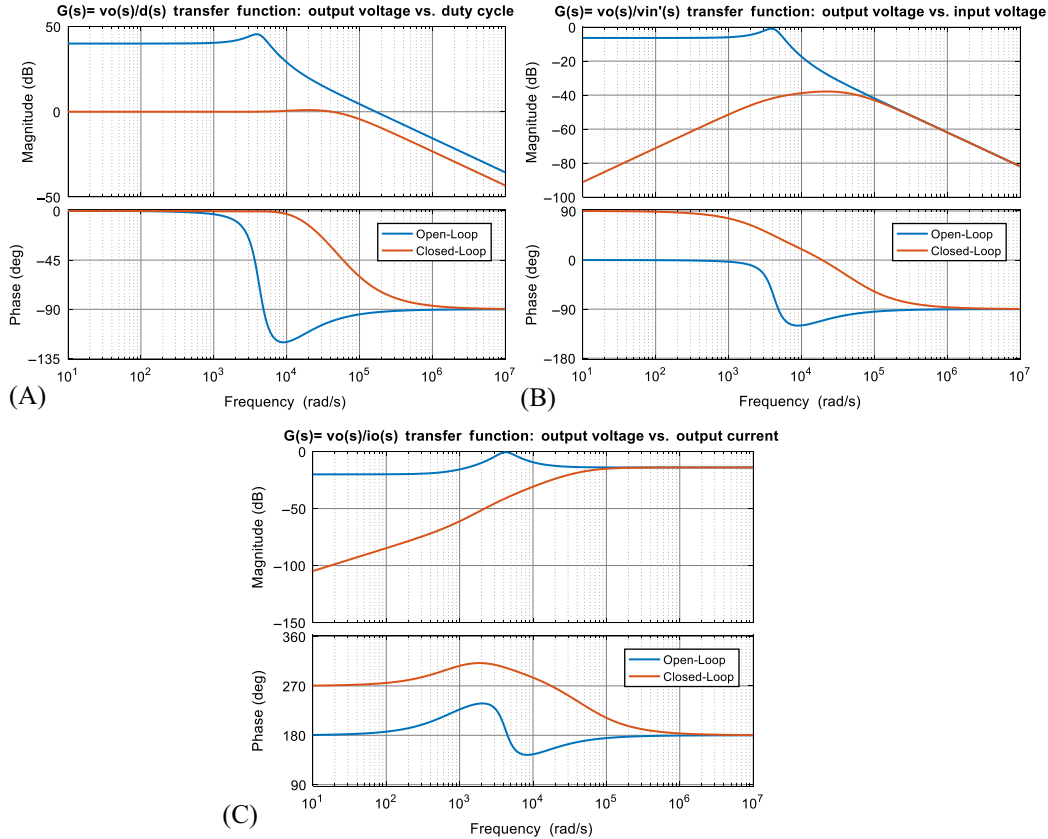


FIG. 3.4 Bode plot of open-loop and closed-loop transfer functions. (A) Control-to-output transfer function, (B) input-to-output transfer function, and (C) output impedance.

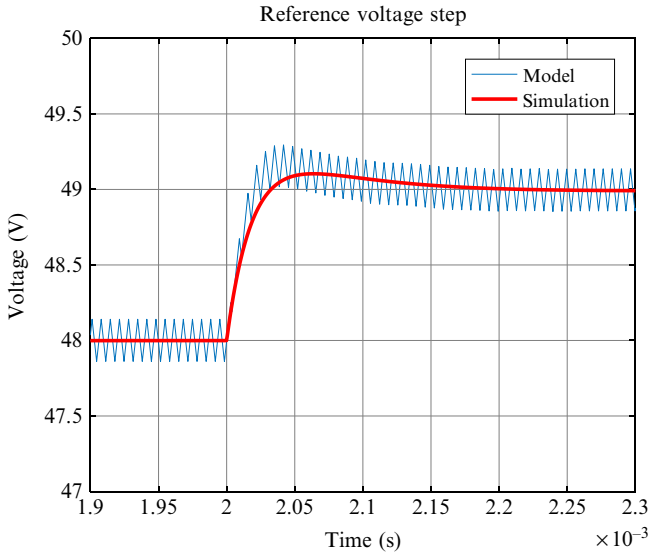


FIG. 3.5 The output voltage reference is varied from 48 to 49 V.

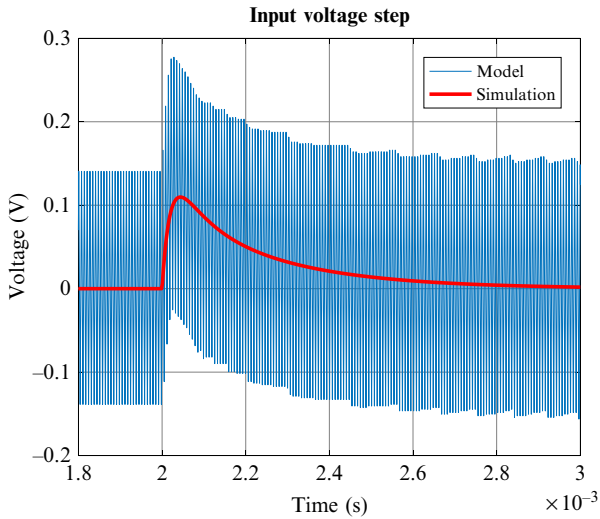


FIG. 3.6 The input voltage is step-changed from 100 to 110V at 2ms.

3.2.2 Small-Signal Modeling of Boost DC-DC Converter

Suppose the Boost converter is operating in the continuous current mode (CCM). When S is turned on, the state equations are

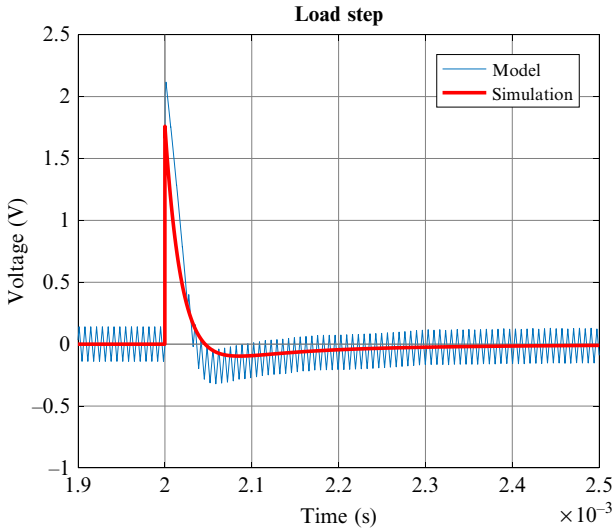


FIG. 3.7 The load is changed from 20 to 10 A at 2 ms.

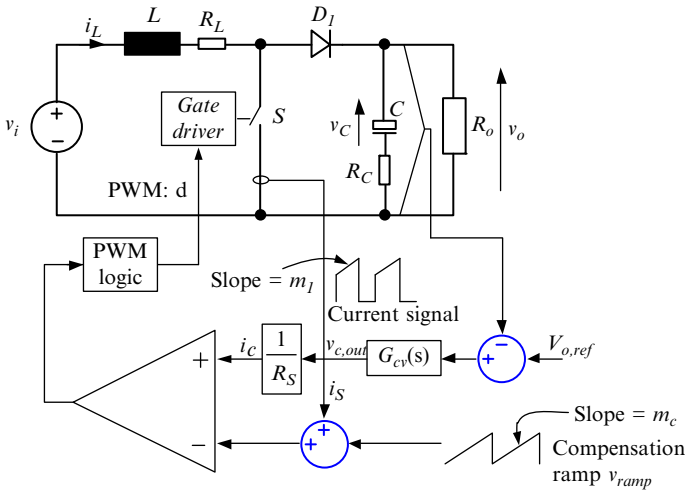


FIG. 3.8 A boost converter with current-mode control.

$$\begin{cases} L \frac{d}{dt} i_L = v_i - i_L R_L \\ C \frac{d}{dt} v_C = -\frac{v_o}{R_o} \end{cases} \quad (3.12)$$

When S is turned off, the diode D_1 is freewheeling; then the state equations are

$$\begin{cases} L \frac{d}{dt} i_L = v_i - i_L R_L - v_o \\ C \frac{d}{dt} v_C = i_L - \frac{v_o}{R_o} \end{cases} \quad (3.13)$$

According to Eqs. (3.12), (3.13), the average model can be obtained as,

$$\begin{cases} L \frac{d}{dt} \bar{i}_L = \bar{v}_i - \bar{i}_L R_L - (1 - \bar{d}) \bar{v}_o \\ C \frac{d}{dt} \bar{v}_C = (1 - \bar{d}) \bar{i}_L - \frac{\bar{v}_o}{R_o} \end{cases} \quad (3.14)$$

where d is the duty ratio of the boost converter, and \bar{x} is the average value of x ($x = i_L, v_i, d, v_o, v_C$) in a switching cycle. As seen in Fig. 3.8, it is easy to acquire

$$\bar{v}_o = \bar{v}_C + R_C C \frac{d}{dt} \bar{v}_C \quad (3.15)$$

Then, by applying small signal perturbations to Eqs. (3.14), (3.15), it is gained

$$\begin{cases} L \frac{d}{dt} (\bar{I}_L + \tilde{i}_L) = (\bar{V}_i + \tilde{v}_i) - (\bar{I}_L + \tilde{i}_L) R_L - (1 - \bar{D} - \tilde{d}) (\bar{V}_o + \tilde{v}_o) \\ C \frac{d}{dt} (\bar{V}_C + \tilde{v}_C) = (1 - \bar{D} - \tilde{d}) (\bar{I}_L + \tilde{i}_L) - \frac{\bar{V}_o + \tilde{v}_o}{R_o} \\ \bar{V}_o + \tilde{v}_o = \bar{V}_C + \tilde{v}_C + R_C C \frac{d}{dt} (\bar{V}_C + \tilde{v}_C) \end{cases} \quad (3.16)$$

Extract the DC items in Eq. (3.16), it is obtained

$$\begin{cases} 0 = \bar{V}_i - \bar{I}_L R_L - (1 - \bar{D}) \bar{V}_o \\ 0 = (1 - \bar{D}) \bar{I}_L - \frac{\bar{V}_o}{R_o} \\ \bar{V}_o = \bar{V}_C \end{cases} \quad (3.17)$$

By removing the DC and high-order AC items in Eq. (3.16), it is acquired

$$\begin{cases} L \frac{d}{dt} \tilde{i}_L = \tilde{v}_i - \tilde{i}_L R_L - (1 - \bar{D}) \tilde{v}_o + \tilde{d} \bar{V}_o \\ C \frac{d}{dt} \tilde{v}_C = (1 - \bar{D}) \tilde{i}_L - \tilde{d} \bar{I}_L - \frac{\tilde{v}_o}{R_o} \\ \tilde{v}_o = \tilde{v}_C + R_C C \frac{d}{dt} \tilde{v}_C \end{cases} \quad (3.18)$$

By performing Laplace transform to Eq. (3.18), it is obtained

$$\begin{cases} sL\tilde{i}_L(s) = \tilde{v}_i(s) - \tilde{i}_L(s)R_L - (1-\bar{D})\tilde{v}_o(s) + \tilde{d}(s)\bar{V}_o \\ sC\tilde{v}_C(s) = (1-\bar{D})\tilde{i}_L(s) - \tilde{d}(s)\bar{I}_L - \frac{\tilde{v}_o(s)}{R_o} \\ \tilde{v}_o(s) = \tilde{v}_C(s) + sR_C C\tilde{v}_C(s) \end{cases} \quad (3.19)$$

Then, Eq. (3.20) can be derived from Eq. (3.19), and the control to output voltage transfer function of the open-loop boost converter is obtained as shown in Eq. (3.21).

$$\tilde{v}_o(s) = \frac{\frac{1+sR_C C}{1-\bar{D}}\tilde{v}_i(s) + \frac{1+sR_C C}{(1-\bar{D})^2}\bar{V}_i \left[1 - \frac{sL}{R_o(1-\bar{D})^2} \right] \tilde{d}(s)}{s^2 \frac{LC}{(1-\bar{D})^2} + s \left[\frac{L+R_L R_o C}{R_o(1-\bar{D})^2} + R_C C \right] + 1} \quad (3.20)$$

$$G_{d2v_o} = \left. \frac{\tilde{v}_o(s)}{\tilde{d}(s)} \right|_{\tilde{v}_i(s)=0} = \frac{\frac{1+sR_C C}{(1-\bar{D})^2}\bar{V}_i \left[1 - \frac{sL}{R_o(1-\bar{D})^2} \right]}{s^2 \frac{LC}{(1-\bar{D})^2} + s \left[\frac{L+R_L C}{(1-\bar{D})^2} + R_C C \right] + 1} \quad (3.21)$$

Fig. 3.9 shows the peak current control of the boost converter, where the switch current i_S instead of the inductor current i_L is applied to compare with the reference i_c that is generated by the voltage compensator. Moreover, in order to increase the damping and mitigate the subharmonic caused by the peak current control, a slope m_c is added into i_S before compared with i_c , as illustrated in Figs. 3.8 and 3.9. The design of m_c will be demonstrated in the following section. By solving the simple trigonometry in Fig. 3.9, it is obtained

$$\bar{i}_L = i_c - m_c \bar{d}T_s - \frac{m_1}{2} \bar{d}T_s \quad (3.22)$$

$$m_1 = \frac{v_i}{L} \quad (3.23)$$

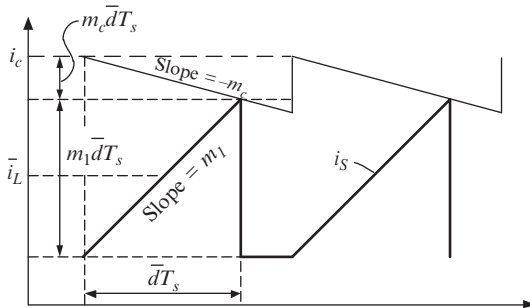


FIG. 3.9 The schematic diagram of peak current control.

By substituting Eq. (3.23) and then applying small-signal perturbation to Eq. (3.22), it is acquired

$$\bar{i}_L + \tilde{i}_L = \bar{i}_c + \tilde{i}_c - m_c (\bar{D} + \tilde{d}) T_s - \frac{\bar{V}_i + \tilde{v}_i}{2L} (\bar{D} + \tilde{d}) T_s \quad (3.24)$$

By removing the DC and high-order AC components in Eq. (3.24), it is gained

$$\tilde{i}_L = \tilde{i}_c - m_c \tilde{d} T_s - \frac{\bar{V}_i \tilde{d} + \bar{D} \tilde{v}_i}{2L} T_s \quad (3.25)$$

By performing Laplace transformation to Eq. (3.25), it is obtained

$$\tilde{i}_L(s) = \tilde{i}_c(s) - m_c \tilde{d}(s) T_s - \frac{\bar{V}_i \tilde{d}(s) + \bar{D} \tilde{v}_i(s)}{2L} T_s \quad (3.26)$$

According to Eqs. (3.19), (3.26), it can be acquired

$$\tilde{v}_o(s) = \frac{G_{NC}(s) \tilde{v}_i(s) + G_{IC}(s) \tilde{i}_c(s)}{\Delta(s)} \quad (3.27)$$

where

$$G_{NC}(s) = (1 - \bar{D}) R_o \left[\frac{s \bar{D} T_s}{2(1 - \bar{D})^2 R_o} + \frac{1}{(1 - \bar{D})^2 R_o} - \frac{\bar{D} T_s}{2L} + \left(1 + \frac{2m_c}{\bar{V}_i} \right) \frac{(1 - \bar{D}) T_s}{2} \right] \quad (3.28)$$

$$G_{IC}(s) = (1 - \bar{D}) R_o (1 + s R_C C) \left[1 - \frac{sL}{(1 - \bar{D})^2 R_o} \right] \quad (3.29)$$

$$\begin{aligned} \Delta(s) &= s^2 L (R_o + R_C) C (1 - \bar{D}) \left(\frac{m_c}{\bar{V}_i} + \frac{1}{2L} \right) T_s \\ &+ s \left\{ \left[L + (1 - \bar{D})^2 R_o R_C C \right] (1 - \bar{D}) \left(\frac{m_c}{\bar{V}_i} + \frac{1}{2L} \right) T_s + (R_o + 2R_C) C \right\} \\ &+ 2 + (1 - \bar{D})^2 R_o (1 - \bar{D}) \left(\frac{m_c}{\bar{V}_i} + \frac{1}{2L} \right) T_s \end{aligned} \quad (3.30)$$

Assuming that the switch current is sampled via a resistor R_S , or the equivalent resistance of the current sensor is R_S , the control to output voltage transfer function of the boost converter with current mode control is obtained

$$G_{v_c, out 2v_o} = \frac{\tilde{v}_o(s)}{\tilde{v}_{c, out}(s)} \Big|_{\tilde{v}_i(s)=0} = \frac{G_{IC}(s)}{\Delta(s) R_S} \quad (3.31)$$

3.2.3 Current-Model Controller Design of Boost DC-DC Converter

A typical issue brought by peak current control is the subharmonics resonance, and it is indicated in Fig. 3.10. As seen, with an improperly designed m_c , the

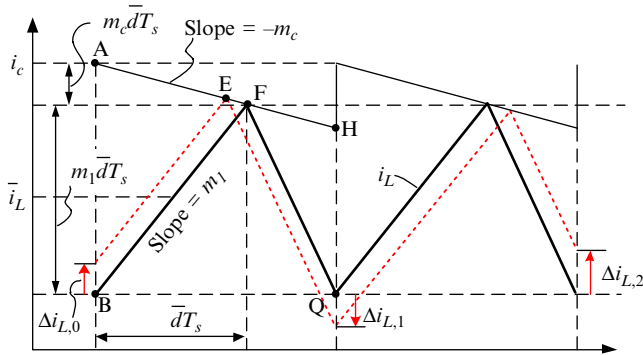


FIG. 3.10 Subharmonic resonance in current mode-controlled boost converter.

inductor current disturbance $\Delta i_{L,0}$ can be amplified after two switching cycles. The impact of m_c on the subharmonics resonance can be revealed by solving the trigonometry in Fig. 3.10, and it is obtained

$$\frac{\Delta i_{L,0}}{AB} = \frac{EF}{AF}, \quad \frac{EF}{FH} = \frac{-\Delta i_{L,1}}{QH} \quad (3.32)$$

Merge the two equations in Eq. (3.32), and it is acquired

$$\Delta i_{L,1} = -\frac{QHAF}{ABFH} \Delta i_{L,0} = -\frac{m_1 \bar{d} T_s - m_c (1 - \bar{d}) T_s}{(m_1 + m_c) \bar{d} T_s} \frac{\bar{d}}{1 - \bar{d}} \Delta i_{L,0} \quad (3.33)$$

To avoid the subharmonics resonance, it requires

$$|\Delta i_{L,1}| \leq |\Delta i_{L,0}| \quad (3.34)$$

Substitute Eq. (3.33) into Eq. (3.34), it is gained

$$\frac{m_1 \bar{d} T_s - m_c (1 - \bar{d}) T_s}{(m_1 + m_c) \bar{d} T_s} \frac{\bar{d}}{1 - \bar{d}} \leq 0.5 \Rightarrow m_c \geq m_1 \frac{2\bar{d} - 1}{2(1 - \bar{d})} \quad (3.35)$$

Since the minimum value of m_c is zero, the condition to eliminate subharmonics resonance is obtained as Eq. (3.36) by substituting Eq. (3.23) into Eq. (3.35).

$$m_c \geq \begin{cases} 0, & \bar{d} \leq 0.5 \\ \frac{v_i}{L} \frac{2\bar{d} - 1}{2(1 - \bar{d})}, & \bar{d} > 0.5 \end{cases} \quad (3.36)$$

A voltage compensator is designed in this section for a current mode controlled boost converter with the specifications described in Section 3.2.1. Substitute the parameter values into Eq. (3.21), and the characteristics of the transfer function G_{d2v_o} is obtained as below:

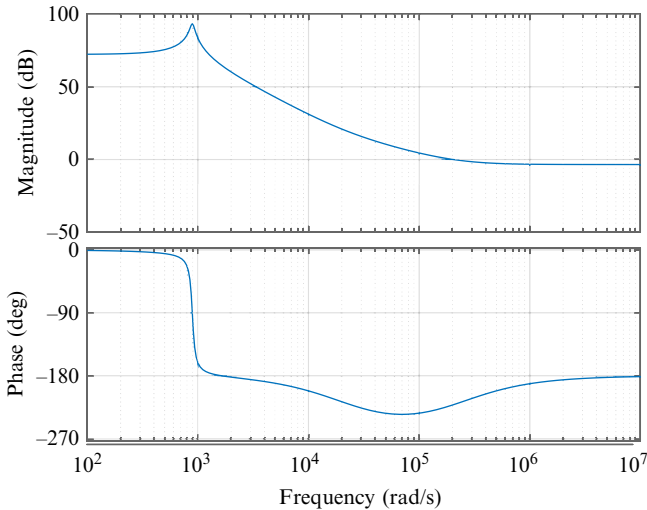


FIG. 3.11 Frequency response of the open-loop boost converter.

DC gain: 4083

Poles: $-39.4 \pm 890j$ rad/s

Zeros: -2.2×10^5 rad/s, 2.19×10^4 rad/s (Right-Half-Plane, RHP)

Fig. 3.11 shows the frequency response of the open-loop-controlled Boost converter. As seen, the open-loop system has a resonant point, where the phase is decreased sharply to -180° . Thus, if a voltage mode control is applied, a much lower crossover frequency than the resonant frequency is necessary for the voltage compensator to damp the resonance and make the system stable.

Substitute the parameter values into Eq. (3.31), the characteristics of the transfer function $G_{v_{c,out}2v_o}$ are obtained:

DC gain: 62

Poles: -80 rad/s, -1.67×10^5 rad/s

Zeros: -2.2×10^5 rad/s, 2.19×10^4 rad/s (RHP)

Crossover frequency: 4.9×10^3 rad/s

Phase margin: 78°

where m_c is set as Eq. (3.37) according to the subharmonics resonance mitigation condition in Eq. (3.36), and a 20% safety margin is applied.

$$m_c = 1.2 \frac{v_i}{L} \frac{2\bar{d} - 1}{2(1 - \bar{d})} \quad (3.37)$$

Fig. 3.12 shows the frequency response of the uncompensated boost converter with current-mode control. As seen, the resonant point does not exist

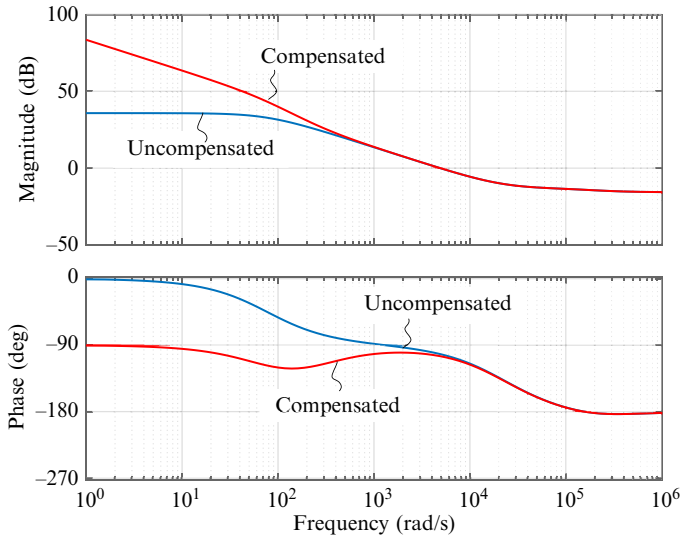


FIG. 3.12 Frequency responses of the current-model-controlled boost converter with and without compensation.

any more compared with Fig. 3.11. To realize an infinite DC gain for nonzero steady-state error tracking, a proportional + integral (PI) voltage compensator is used, as shown

$$G_{cv}(s) = K_p \frac{s + \frac{K_i}{K_p}}{s} \quad (3.38)$$

The crossover frequency of the uncompensated system is 4.9×10^3 rad/s which is around 1/64 of the switching frequency (50kHz). Normally, the crossover frequency can be set to around 1/10 of the switching frequency to have a reasonably high bandwidth. Therefore, the PI compensator can be designed to increase the crossover frequency of the system. But the uncompensated system has a -7 dB constant gain and -180° phase at high-frequency band due to the RHP zero, and the corner frequency to the high-frequency band is 2.19×10^4 rad/s (RHP zero) which is only four times the crossover frequency. Thus, if the crossover frequency is increased by the PI compensator, then the gain at the high-frequency band will also be increased and thereby the system may lose its stability. It is decided to keep the crossover frequency and phase margin of the system by setting a 0-dB gain at the high-frequency band in the PI compensator. Thus, we can obtain $K_p = 1$.

As known, the PI compensator will have a -45° phase at its corner frequency. To avoid a significant influence on the phase margin of the system, the corner frequency of the PI compensator is set to 1/15 of the crossover frequency of the system, i.e.,

$$K_i/K_p = 4.9/15 \text{ krad/s} \quad (3.39)$$

Thus, it is gained $K_i = 327$ and

$$G_{cv}(s) = 1 + \frac{327}{s} \quad (3.40)$$

3.2.4 Simulation Results of the Case Study

Figs. 3.13 and 3.14 show the simulation results of the specific case study. Without the slope compensations, subharmonics appear when m_c is equal to $0.8m_{c0}$. By adding a slope compensation, the subharmonics can be eliminated. The overshoot and undershoot of the Boost converter output voltage is limited to a relatively low level under step load changes occur, as shown in Fig. 3.14. The results imply a proper current controller for the Boost converter is achieved.

3.3 TIME-DOMAIN CONTROL OF BASIC DC-DC CONVERTERS

The controllers of DC-DC converters are dominantly designed with small-signal linearization techniques in frequency domain, as discussed in Sections 3.1 and 3.2. However, DC-DC converters with PWM switching are highly nonlinear systems, and their large-signal characteristics will behave differently from that predicted by small-signal design approaches. To overcome the limitations, various time-domain control methods have been proposed. One major class of them is the switching surface control (i.e., boundary control). The concept is to determine the time sequence to turn on/off switches according to certain constrains, namely, switching surfaces [1]. This section is dedicated to a case study to illustrate the basic concept of a generic second-order boundary

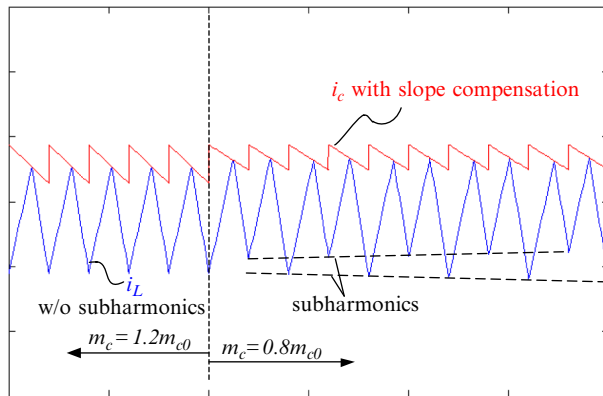


FIG. 3.13 Simulation results to show the impact of the slop compensation on the subharmonics

resonance in peak current control $\left(m_{c0} = \frac{v_i}{L} \frac{2T-1}{2(1-d)}\right)$.

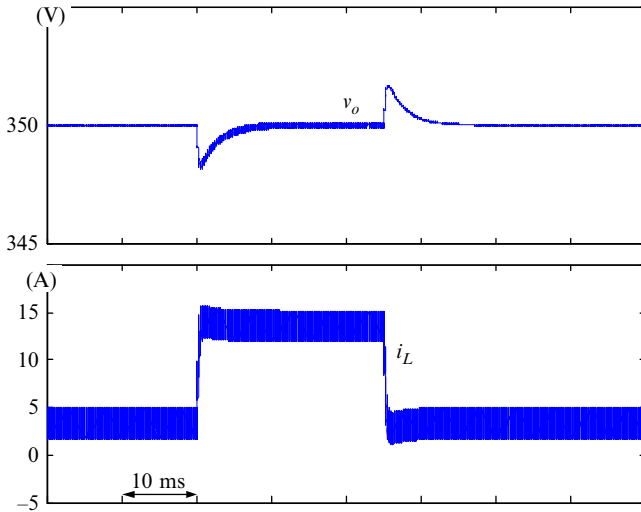


FIG. 3.14 Simulation results to show the dynamic performance of the system during load step.

control method that can be applicable to both Buck-type (i.e., minimum phase system) and Boost type (i.e., nonminimum phase system) converters. Parts of this section are based on what have been discussed in Ref. [1]. The following discussions are based on a specific example of Buck-Boost converter. It should be noted that the method is applicable to all kinds of basic DC-DC converters (i.e., Buck converter, Boost converter, Buck-Boost converter, Ćuk converter, and SEPIC).

3.3.1 Specifications of the Buck-Boost DC-DC Converter

Fig. 3.15 shows the circuit diagram of a Buck-Boost converter. In a specific case study, the parameters are as: output power 190 W, input voltage $v_{in} = 48$ V, and

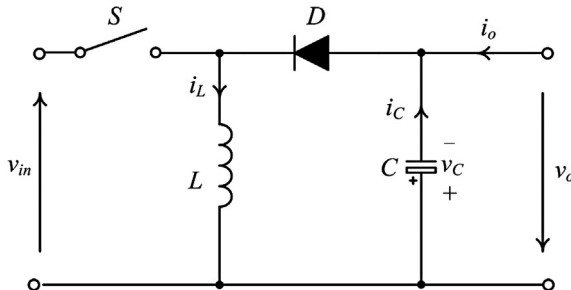


FIG. 3.15 Circuit diagram of a Buck-Boost converter.

output voltage $v_o = 48$ V (according to the polarity definition shown in Fig. 3.15). The inductor $L = 0.36$ mH and the capacitor $C = 150$ μ F.

3.3.2 Concept of Generic Second-Order Boundary Control

Second-order switching surfaces are proposed for buck converter [2] as shown in Fig. 3.16. The nonlinear switching surfaces approximately follow the on/off state trajectories of Buck converter. i_L and v_C are the output inductor current and output capacitor voltage of Buck converter, respectively. Therefore, the parameters used in the control law are well defined, and the converter can revert to steady state after two switching actions. A single control law is applicable for buck converter operating in both continuous conduction mode (CCM) and discontinuous conduction mode (DCM). The control methods are named as boundary control with second switching surface [2]. However, one remaining fundamental issue which poses great challenges is that the same concept cannot be easily applied to converters with nonminimum-phase characteristics [1]. It is difficult to formulate a simple switching surface on the state-plane for a converter with state trajectories in spiral shape, such as Boost converter and Buck-Boost Converter, as discussed in Ref. [1].

To handle the above fundamental issue in switching surface control and incorporate the advantages of the boundary control with second-order switching surface which has been applied on buck converter, a uniform second-order switching surface is proposed. It extends the control state variables (i.e., inductor

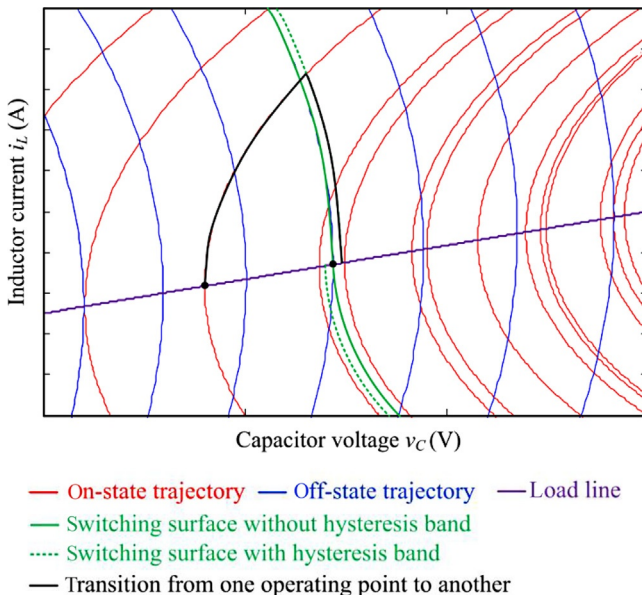


FIG. 3.16 Switching surface control method for Buck converter.

currents and capacitor voltages) in previously proposed switching surface controllers to arbitrary direct or indirect control variables, namely, x and y . Consequently, the relationships between x and y in all basic DC-DC converters are the same as that of i_L - v_C in buck converter. Therefore, the switching surfaces of different kind of converters can be easily defined on a Cartesian x - y plane. x and y have the same properties as those of inductor current and capacitor voltage, respectively, in buck converter, implying that

$$\frac{dy}{dx} = 2k_s(x - x_{ref}) \tag{3.41}$$

where k_s is state trajectory parameter related with the slope of x and x_{ref} is the reference value.

With the aid of Fig. 3.17 according to Eq. (3.41), the approximated on-state trajectory $\text{Traj}|_{on}$ and off-state CCM trajectory $\text{Traj}|_{off}$ can be expressed, respectively, as follows

$$\text{Traj}|_{on} = y(t) - y(t_0) - k_{s1} \left\{ [x(t) - x_{ref}]^2 - [x(t_0) - x_{ref}]^2 \right\} = 0 \tag{3.42}$$

$$\text{Traj}|_{off} = y(t) - y(t_2) - k_{s2} \left\{ [x(t) - x_{ref}]^2 - [x(t_2) - x_{ref}]^2 \right\} = 0 \tag{3.43}$$

where t_0 and t_2 are the turn on/off instants, respectively, k_{s1} is the trajectory parameter during on-state period, and k_{s2} is that during off-state CCM period. It is noted that $k_{s1} > 0$ and $k_{s2} < 0$. In DCM, after the x reaches zero, the trajectory moves along the y -axis, $x = 0$, and the corresponding trajectory parameter $k_{s3} = 0$ during this interval.

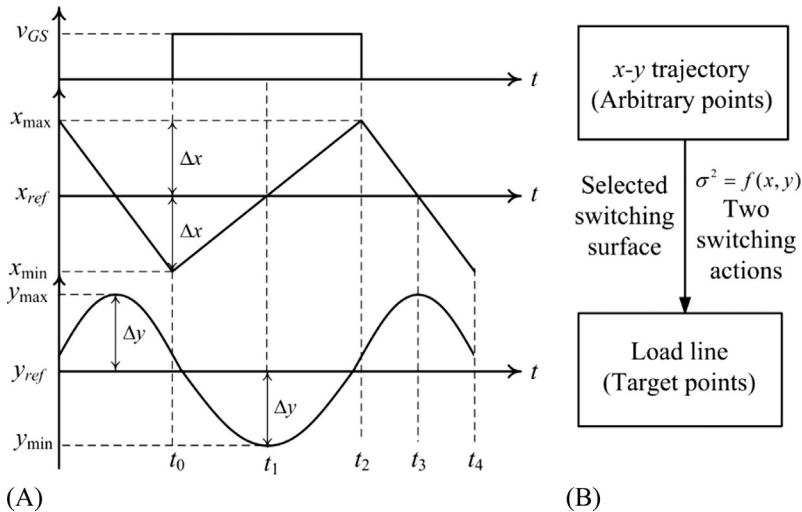


FIG. 3.17 Principle of boundary control with uniform second-order switching surface: (A) control variables and (B) control law.

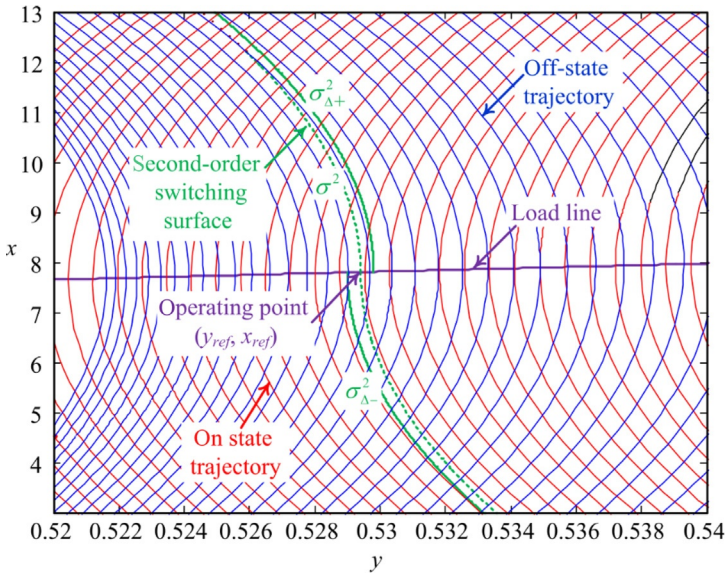


FIG. 3.18 Typical trajectories, load line, and switching surface of basic DC-DC converters on the x - y plane.

Fig. 3.18 presents the generic switching surfaces, load line, and ideal on/off state-trajectories of basic DC-DC converters on x - y plane. The trajectories are plotted by first solving on- and off-state space equations of specific converter with different initial conditions and then mapping the state variables i_L and v_C to x and y , respectively. It is the ideal state trajectories which can be approximated by Eqs. (3.42), (3.43).

As discussed in Ref. [2], the ideal second-order switching surface σ^2 should pass through the target operating point (y_{ref}, x_{ref}) , and exactly along the approximated on-state trajectory when x is below the load line, and the off-state trajectory when x is above the load line. By transforming the i_L - v_C state plane to the Cartesian x - y plane, a well-defined uniform second-order switching surface σ^2 can be obtained as shown in Fig. 3.18. It approximately follows the ideal on-state trajectory and off-state trajectory when the state is below and above the load line, respectively, implying a high velocity to revert to the target operating point from arbitrary operating points.

The switching instants are determined by predicting the operating point at t_1 and t_3 as shown in Fig. 3.17. By putting $y(t) = y_{ref}$, $x(t) = x_{ref}$, $y(t_0) = y$, and $y(t_2) = y$ into Eqs. (3.42), (3.43), respectively, a general form of the switching surface is given by

$$\sigma^2 = (y - y_{ref}) - k(x - x_{ref})^2 \quad (3.44)$$

where σ^2 is the uniform second-order switching surface and k is the control parameter and can be expressed as follows for an ideal second-order switching surface

$$k = k_{s1} \left[\frac{1 - \text{sgn}(x - x_{ref})}{2} \right] + k_{s2} \left[\frac{1 + \text{sgn}(x - x_{ref})}{2} \right] \quad (3.45)$$

k can be of other values, which affect the stability and trajectory velocity along the switching surface as discussed in Ref. [1]. In the following analysis, k_1 and k_2 are defined as general control parameters for turn-on and turn-off switching actions, respectively. Practically, to avoid chattering phenomenon, a modified switching surface σ_{Δ}^2 is derived by adding a hysteresis band $2\Delta y$ as shown in Fig. 3.18 into Eq. (3.44), resulting in

$$\sigma_{\Delta}^2 = \begin{cases} \sigma_{\Delta-}^2 = y - y_{ref} - k_1 (x - x_{ref})^2 + \Delta y & (x < x_{ref}) \\ \sigma_{\Delta+}^2 = y - y_{ref} - k_2 (x - x_{ref})^2 - \Delta y & (x > x_{ref}) \end{cases} \quad (3.46)$$

where $\sigma_{\Delta-}^2$ and $\sigma_{\Delta+}^2$ are the uniform second-order switching surface below and above load line.

Therefore, the uniform control law for the basic DC-DC converters is formulated as follows. The switch S is turned on if

$$y(t) - k_1 (x - x_{ref})^2 - (y_{ref} - \Delta y) \leq 0 \quad \text{and} \quad x(t) < x_{ref} \quad (3.47)$$

S is turned off if

$$y(t) - k_2 (x - x_{ref})^2 - (y_{ref} + \Delta y) \geq 0 \quad \text{and} \quad x(t) > x_{ref} \quad (3.48)$$

For Buck converter, Boost converter, Buck-Boost converter, Ćuk converter, and SEPIC, the respective x and y can be derived, as discussed in detail in Ref. [1]. Section 3.3.3 will take Buck-Boost converter as an example to derive the x and y .

3.3.3 Second-Order Boundary Controller Design for Buck-Boost Converter

Fig. 3.19 shows the operation modes of Buck-Boost converter. x , y , k_1 , and k_2 are derived by the following steps:

Step 1: Derivation of the load line. The load line is derived by considering the average steady-state inductor current $i_{L,ref}$. For the Buck-Boost converter,

$$i_{L,ref} = \frac{v_o i_o}{v_{in}} + i_o \quad (3.49)$$

where v_{in} is the input voltage, and v_o and i_o are the output voltage and current, respectively.

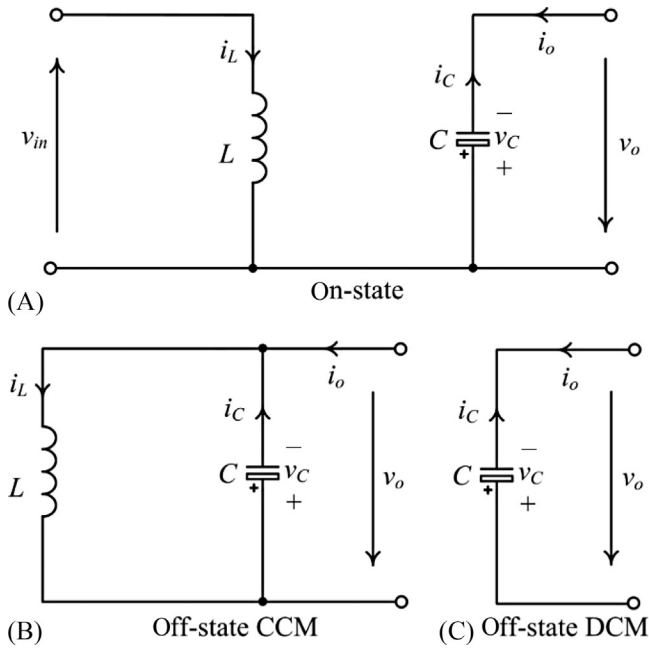


FIG. 3.19 Operation modes of buck-boost converter.

Step 2: Determination of x , y , and k_{s1} . For the Buck-Boost converter, the control variable x is first selected as the inductor current i_L . As shown in Fig. 3.19A, during on-state interval,

$$\frac{dv_o}{di_L} = -\frac{Lv_o}{RCv_{in}} \quad (3.50)$$

where L and C are the inductor and output capacitor, respectively, and R is the equivalent load resistance.

By using Eq. (3.41), it can be shown that

$$y = 2k_1 \int (i_L - i_{L,ref}) di_L = \frac{2k_1}{L} \left(\frac{1}{2} L i_L^2 + \frac{1}{2} C v_o^2 + C v_{in} v_o \right) \quad (3.51)$$

Hence, y can be chosen as

$$y = \frac{1}{2} L i_L^2 + \frac{1}{2} C v_o^2 + C v_{in} v_o \quad (3.52)$$

$$k_1 = \frac{L}{2} \quad (3.53)$$

Step 3: Determination of k_2 . As shown in Fig. 3.19B, during off-state interval,

$$\frac{dy}{di_L} = \frac{dy}{dt} \frac{dt}{di_L} = -\frac{Lv_{in}}{v_o} (i_L - i_{L,ref}) \tag{3.54}$$

$$k_{s2} = -\frac{Lv_{in}}{2v_o} \tag{3.55}$$

Step 4: Calculation of y_{ref} . Based on Eqs. (3.49), (3.52),

$$y_{ref} = \frac{1}{2}L \left(\frac{v_o i_o}{v_{in}} + i_o \right)^2 + \frac{1}{2}C v_{o,ref}^2 + C v_{in} v_{o,ref} \tag{3.56}$$

Step 5: Formation of the control law. According to Eqs. (3.47), (3.48), the switching criterion is described as follows. The switch S is turned on if

$$y(t) - k_1 (i_L - i_{L,ref})^2 - (y_{ref} - \Delta y) \leq 0 \text{ and } i_L(t) < i_{L,ref} \tag{3.57}$$

S is turned off if

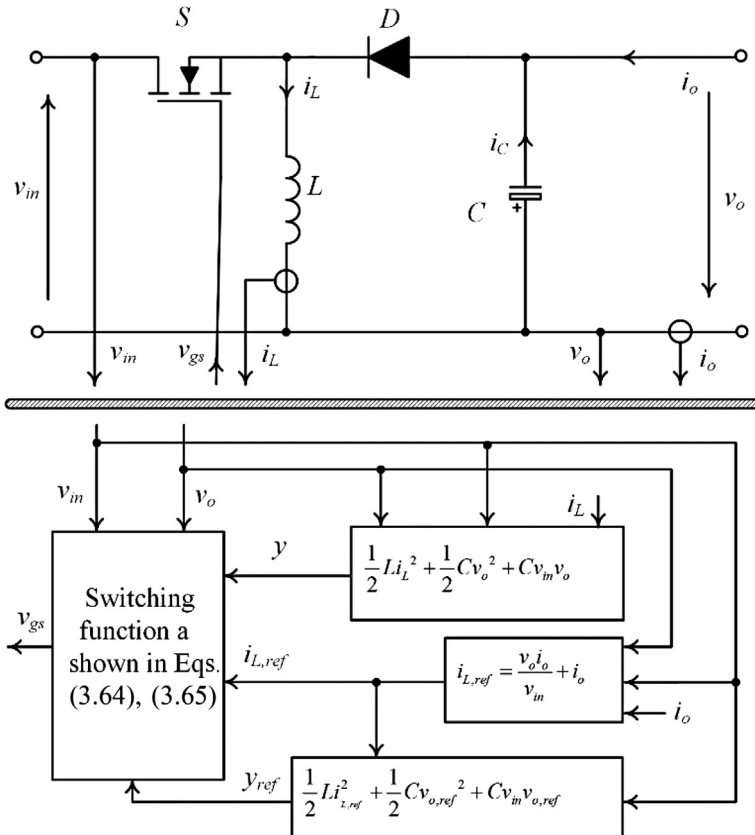


FIG. 3.20 Block diagram of the proposed controller for Buck-Boost converter.

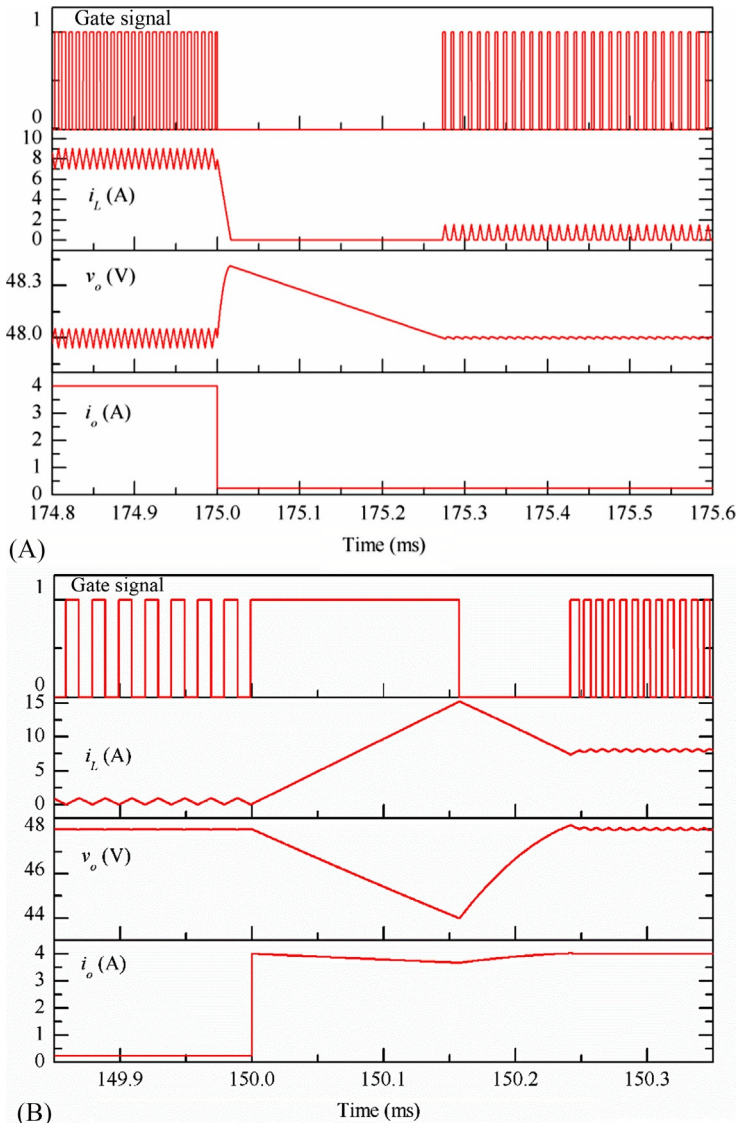


FIG. 3.21 Simulation results of Buck-Boost converters with the proposed controller. (A) Load change from 12 to 200 Ω (CCM to DCM) and (B) Load change from 12 to 200 Ω (CCM to DCM).

$$y(t) - k_2(i_L - i_{L,ref})^2 - (y_{ref} + \Delta y) \geq 0 \quad \text{and} \quad i_L(t) > i_{L,ref} \quad (3.58)$$

Step 6: Implementation of control law. Based on the above derivations, the block diagram of the controller for the Buck-Boost converter is shown in Fig. 3.20.

3.3.4 Simulation Results of the Case Study

Simulations have been performed for the Buck-Boost converter with the specifications described in [Section 3.3.1](#). The results are shown in [Fig. 3.21](#). The converter can revert to steady state by two switch actions after being exposed to large disturbances.

REFERENCES

- [1] H. Wang, *New Energy-Efficient High-Voltage DC-DC Power Conversion Technology*, City University of Hong Kong, Hong Kong, Mar. 2012.
- [2] K.S. Leung, H.S.H. Chung, "Derivation of a second-order switching surface in the boundary control of buck converters," *IEEE Power Electron. Lett.* 2 (2) (2004) 63–67.